Chapter 8

Ultrashort Pulse Generation in Ce:LiCAF Ultraviolet Laser

Marilou Cadatal-Raduban, Minh Hong Pham, Luong Viet Mui, Nguyen Dai Hung and Nobuhiko Sarukura

Additional information is available at the end of the chapter

http://dx.doi.org/10.5772/intechopen.73501

Abstract

Transient cavity method used to generate ultrashort laser pulses in dye lasers is extended to a solid-state gain medium. Numerical simulations are performed to investigate the spectro-temporal evolution of broadband ultraviolet (UV) laser emission from Ce^{3+}-doped $LiCaAlF_6$ (Ce:LiCAF), which is represented as a system of two homogeneous broadened singlet states. By solving the rate equations extended to multiple wavelengths, the appropriate cavity length and Q-factor for optimal photon cavity decay time and pumping energy that will generate resonator transients is determined. Formation of resonator transients could generate picosecond UV laser pulses from a Ce:LiCAF crystal pumped by the fourth harmonics (266 nm) of a Nd:YAG laser. Numerical simulations indicate that a 1-mol% Ce^{3+}-doped LiCAF crystal that is 1-mm long can generate a single picosecond pulse. This is accomplished by using a low Q (output coupler reflectivity of 10%), short cavity (cavity length of 2 mm) laser oscillator. Ultrashort pulses can also be generated using other rare earth-doped fluoride laser materials using this technique.

Keywords: numerical simulation, ultrashort pulse, ultraviolet, resonator transient, Ce:LiCAF crystal

1. Introduction

Tunable ultrashort-pulsed laser emission in the ultraviolet (UV) region is highly sought after because of its numerous applications in many fields of science and technology [1, 2]. Ultrashort pulses are necessary for controlling ultrafast chemical processes [1], probing fast physical and chemical processes [3, 4], and investigating the relaxation of charge carriers in conductors [5],

to name a few. On the other hand, UV lasers have many applications in various fields such as surface structuring [6–8], micromachining [9], remote sensing [10], spectroscopy and imaging [11]. An important advantage of having ultrashort pulses in the UV wavelength region is its ability to modify material properties only within the laser focus where the peak power is high. This feature is especially critical in micromachining [12]. Ultrashort UV pulses also permit outstanding temporal resolutions for pump-probe experiments [13]. Available light sources that satisfy these requirements are limited, despite the many applications. Excimer lasers can emit UV wavelengths, but these are bulky and cumbersome to maintain [14, 15]. UV laser emission using frequency conversion in nonlinear crystals is well established but is complex, has limited spectral bandwidth, non-tunable, and has low conversion efficiency. In contrast, high-power, all-solid-state UV lasers are highly regarded for simplicity in operation and maintenance. Hence, there is a great deal of interest for developing all-solid-state UV lasers.

Cerium ion (Ce^{3+})-doped wide band gap fluorides have been the most successful tunable solid-state laser media in the UV region. Direct UV emission has been reported from Ce^{3+}-doped $YLiF_4$, LaF_3, $LiLuF_4$, $LiCaAlF_6$, and $LiSrAlF_6$ crystals [16–23]. Among these known UV laser crystals, Ce^{3+}-doped lithium calcium hexafluoroaluminate (Ce^{3+}:$LiCaAlF_6$ or Ce:LiCAF) is the most prominent and successful solid-state gain medium for amplifying short UV pulses as well as for generating ultrashort UV pulses because it is highly transparent, has low excited state absorption, not prone to color center formation and therefore tolerant to laser-induced damage. Most importantly, it is absorbing at around 266 nm, which makes the fourth harmonics of readily-available Nd:YAG lasers an ideal excitation source. It also has sufficiently large effective gain cross-section of 6.0×10^{-18} cm^2 that is favorable for oscillators, and a high saturation fluence of 115 mJ/cm^2. Lastly, it has broad tunability from 280 to 325 nm and enough bandwidth to generate 3-fs pulses [2, 20–22, 24–30].

Direct generation of tunable UV short-pulses using solid-state gain media, such as Ce:LiCAF, is not as straight forward as using near IR tunable solid-state laser media, such as Ti:sapphire, due to the difficulty of obtaining continuous wave (CW) laser operation. As a result, Kerr lens mode-locking schemes that utilize spatial or temporal Kerr type nonlinearity are a real challenge in the UV region [31]. The lifetime of the upper energy level of Ce:LiCAF is about 25 ns, which is too short to directly generate tunable UV short-pulses. Therefore, high pump power densities are required to achieve CW and mode-locked operation [32]. Moreover, the cavity lengths of the pump and the Ce:LiCAF laser oscillator have to be matched for synchronous mode locking [33]. A typical oscillator in mode-locking schemes also uses a four-mirror z-fold cavity, which means that reducing losses in the laser cavity is also crucial. On the other hand, the transient cavity method is a simpler means of generating tunable UV ultrashort pulses because it only utilizes the usual two-mirror laser oscillator. Pulse shortening by resonator transients has been demonstrated in dye lasers where laser pulse durations that are an order of magnitude shorter than the pump pulse have been obtained [34–36]. This book chapter discusses numerical simulations that extend the resonator transient technique to solid-state gain media. Since formation of resonator transients that lead to picosecond pulses depend on the cavity length and the Q-factor of the laser oscillator cavity, numerical simulations are carried out to investigate the decay time of the photons within the laser cavity as well as the energy of the picosecond Nd:YAG pump laser that will support the formation of these resonator transients. The technique can be extended to other rare earth-doped fluoride laser materials.

2. Review of cerium ion-doped fluoride crystals

Laser gain media based on wide bandgap fluoride hosts was first proposed as a result of spectroscopic studies on trivalent lanthanides such as neodymium (Nd), cerium (Ce), and thulium (Tm) doped in solid-state hosts [37]. The intense broad band UV fluorescence from 276 to 312 nm observed from Ce^{3+}:LaF_3 and the 288–322 nm fluorescence from Ce^{3+}:LuF_3 were attributed to dipole-allowed 5d to 4f (5d-4f) radiative transition of Ce ions in the LaF_3 and LuF_3 fluoride hosts [38]. Subsequently, the first laser emission from the 5d-4f transition was achieved in 1977 using Ce^{3+}:$YLiF_4$. It emitted at 325.5 nm when it was optically pumped at 249 nm [16]. However, the progress of Ce^{3+}:$YLiF_4$ was limited by poor performance characteristics brought about by an early onset of saturation and roll off in the above-threshold gain and power output as well as a drop in the output for pulse repetition rates above 0.5 Hz. Although lasing from Ce^{3+}:$YLiF_4$ is ground breaking, the existence of solarization or color center formation prevents this material from being of practical use, thereby hindering its further development. In 1980, operation of an optically pumped Ce^{3+}:LaF_3 laser was reported [17]. Limitations of this laser medium include low output power and high lasing threshold. Moreover, the lasing results have not been reproduced. Subsequent experiments on other Ce^{3+}-doped fluorides have not been very successful due to the formation of transitory or permanent color centers. Such color centers were essentially due to absorption of the pump and/or the laser radiation from emitting 5d states leading to the promotion of an electron into the conduction band followed by trapping by impurities or defects [39–43]. Recent investigations, however, showed that by an appropriate choice of activator-matrix complexes and active medium-pump source combinations, efficient tunable lasers using d-f transitions can be created [19, 21, 22, 44]. In 1992, emission from Ce^{3+}:$LiLuF_4$ pumped by a KrF excimer laser was reported. This laser material has almost the same optical properties as Ce^{3+}:$YLiF_4$ but with smaller solarization effect [19]. As a result, slope efficiencies of more than 50% were obtained [45, 46]. Moreover, continuous tunability was achieved from 305 to 333 nm [46]. Subsequently, lasing from Ce^{3+}:$LiCaAlF_6$ (Ce:LiCAF) was reported. This was a milestone not only because Ce:LiCAF can be pumped by the fourth harmonic of a Nd:YAG laser, but also because remarkably, no solarizaion effect was observed

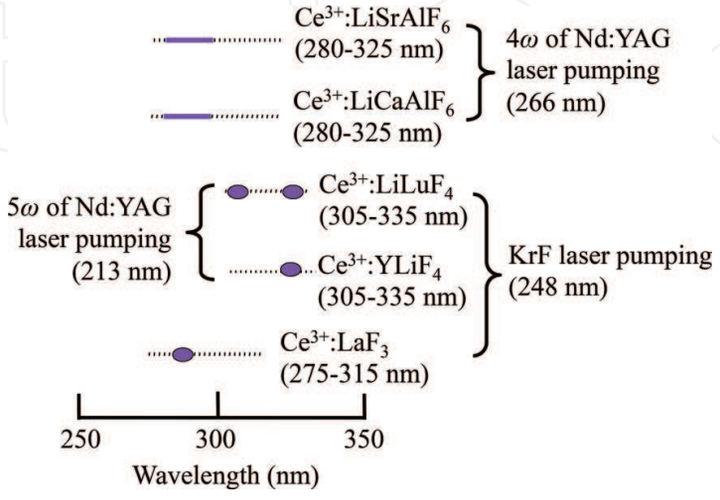

Figure 1. Ce^{3+}-doped lasers for tunable UV radiation. Solid lines and dots indicate the confirmed tunable wavelength region, dotted lines show potential tunable wavelength region.

in this crystal [21, 22]. Following the success of Ce:LiCAF, lasing from Ce^{3+}:$LiSrAlF_6$ was reported. It can also be pumped with the fourth harmonic of a Nd:YAG laser and it has similar laser properties as the Ce:LiCAF crystal [23, 47]. **Figure 1** summarizes the tunable wavelength regions of the five currently known Ce-doped lasers.

Ce:LiCAF has the following advantages over the other known Ce^{3+}-doped fluoride hosts: (1) the strong absorption band at 266 nm would allow direct optical pumping by the fourth harmonics of the Nd:YAG laser; (2) the wide fluorescence band offers a tuning range from the 280 to 320 nm for possible pulse compression; (3) the gain cross-section of Ce:LiCAF (6×10^{-18} cm^2) is high, even higher compared to the Ti:Sapphire. This property is ideal for building a laser resonator; (4) the saturation fluence (~115 mJ/cm^2) of Ce:LiCAF is higher than organic dyes. This is significant when using this crystal in power amplifiers; (5) the nanosecond lifetime of Ce:LiCAF maybe too short to for regenerative amplifications, but this is sufficiently long to allow multi-pass amplification.

3. Cerium ion dopant

Figure 2 shows the energy level structure of Ce^{3+} doped into a fluoride host. The ground state 4f configuration has two energy levels, $^2F_{5/2}$ and $^2F_{7/2}$, which are separated by 0.2793 eV (2253 cm^{-1}). The excited state 5d configuration also has two energy levels, $^2D_{3/2}$ and $^2D_{5/2}$, which are separated by 6.166 eV (49,733 cm^{-1}) and 6.475 eV (52,226 cm^{-1}) from the ground state, respectively. The exact positions of these energy levels would depend on the specific host. Lasing in the UV is based on the electric dipole-allowed interconfigurational 5d-4f transitions. In contrast, conventional trivalent lanthanide laser crystals, such as Nd:YAG, uses the intraconfigurational 4f-4f transition that results to infrared (IR) emission. As a result, UV

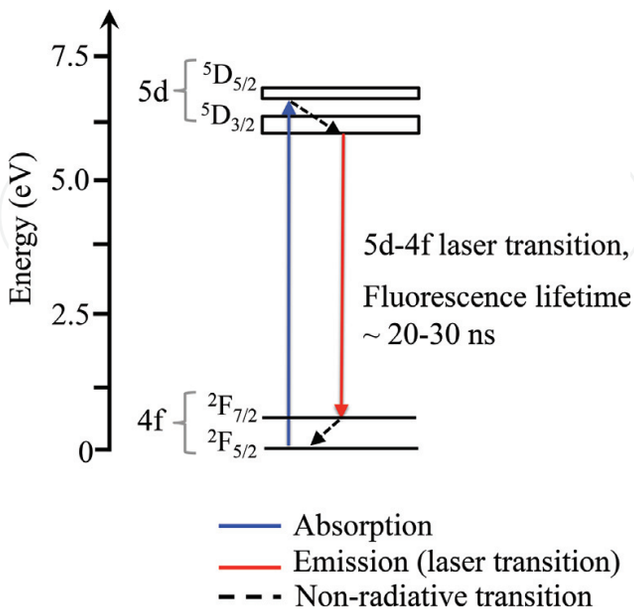

Figure 2. Energy level structure of Ce^{3+} doped into a fluoride host.

fluorescence emission from Ce^{3+}-doped fluoride crystals have smaller radiative lifetimes of a few tens of nanoseconds compared to IR emissions that have lifetimes within hundreds of microseconds. In addition, fluorescence from the 5d-4f transitions is characterized by broad bandwidths and large Stokes shifts. The broad gain bandwidth enables tunability and ultrashort laser pulse generation from Ce^{3+}-activated laser crystals. The large energy gap between the excited state 5d configuration and the 4f ground state configuration laser levels results to low multi-phonon related nonradiative decay. Therefore, quantum efficiencies as high as 90% are expected from Ce^{3+}-activated laser crystals [20, 48].

4. Numerical simulation of the electronic properties of the LiCAF host

LiCAF is a colquiriite-type fluoride with a hexagonal crystal structure belonging to the P-31c space group (group number 163). It is optically a uniaxial crystal with two formula units per unit cell. Six fluorine (F) atoms surround a lithium (Li), calcium (Ca), or aluminum (Al) atom. Each Li, Ca, and Al cation occupies a deformed octahedral site as shown in **Figure 3a**. This structure is also described by an alternative stacking of metallic and fluorine atom layers parallel to the c-axis [49–51]. The fraction coordinates of the representative atoms in the unit cell are shown in **Table 1**.

First-principles density functional theory (DFT) calculations are used to obtain the optimized volume, electronic band structure, total and partial density of states (DOS), and the band gap

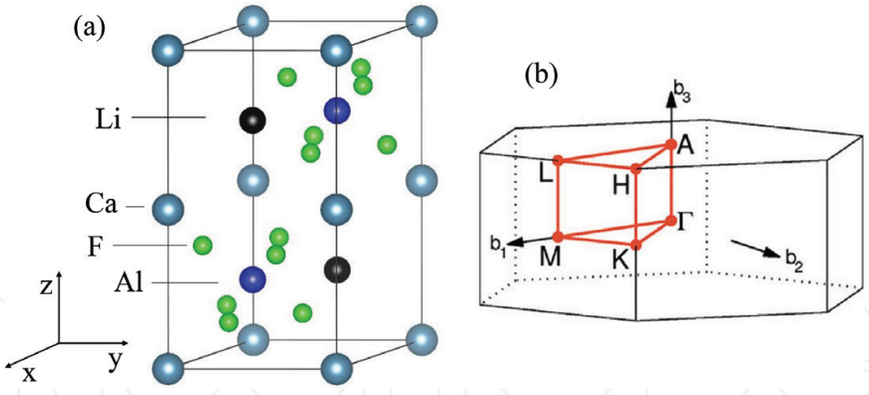

Figure 3. (a) Colquiriite-type structure of LiCAF and (b) first Brillouin zone of the hexagonal unit cell of a LiCAF crystal.

	x	y	z
Li	1/3	2/3	1/4
Ca	0	0	0
Al	2/3	1/3	1/4
F	0.3769	0.0312	0.1435

Table 1. Atomic positions of the LiCAF atoms.

energies of the LiCAF crystal. These calculations employed the projector-augmented wave (PAW) method as implemented within the Vienna Ab Initio Simulation Package (VASP) [52–57], with a plane-wave basis cutoff of 500 eV and a hybrid density functional, which uses the full Perdew-Burke-Ernzerhof (PBE) [58, 59] correlation energy but mixes 65% PBE exchange with 35% exact exchange [60–63]. The initial charge density and wave function was generated using a $3 \times 3 \times 1$ Monkhorst-Pack k-point grid. For the band structure and DOS diagrams, the k-points were chosen following the first Brillouin zone and the path $\Gamma \rightarrow M \rightarrow K \rightarrow A \rightarrow L \rightarrow H$ shown in **Figure 3b** [64].

The electronic band structure of LiCAF along the high symmetry lines of the first Brillouin zone is shown in **Figure 4**. The maximum of the valence band is located at the k-point between M and K while the conduction band minima is at the Γ point. Therefore, LiCAF has an indirect band gap with a band gap energy of 12.23 eV. This result is 3.30% and 10.51% different from the experimentally obtained band gap energies of 12.65 eV and 11.07 eV, respectively [65–67]. **Figure 5** shows the total and partial DOS of LiCAF. The maximum valence band is derived from the fluorine 2p states whereas the aluminum 4 s and fluorine 3 s states contribute to the minimum conduction band.

Excited state absorption (ESA), which is prevalent in rare-earth-doped fluorides operating in the UV region, has been observed in both Ce^{3+}:$LiCaAlF_6$ (Ce:LiCAF) and Ce^{3+}:$LiSrAlF_6$ (Ce:LiSAF). However, experimental investigations reveal that Ce:LiSAF experiences ESA to a greater extent compared to Ce:LiCAF and therefore, the conversion efficiency of a Ce:LiSAF laser is lower. ESA results from an electron being promoted from the 5d excited state configuration of Ce^{3+} to the conduction band of the LiCAF host [24, 68]. Therefore, the onset of ESA strongly depends on the host. If the conduction band minimum of the host is close to the 5d excited state level of the activator ion, then ESA will be greater in this laser material. Similar band structure and DOS calculations performed for LiSAF reveal that the band gap energy of LiSAF is 11.79 eV, which is 0.44 eV smaller than LiCAF [62]. Associated with the strong ESA is color center formation or solarization, which happens due to an electron getting trapped at impurities in the conduction band of the host as shown in **Figure 6** [27]. Under UV excitation, color centers can be created due to solarization. Broad absorption bands in energies other than the band gap then appear as a result of color center-formation. The Ce^{3+} ions that are doped in

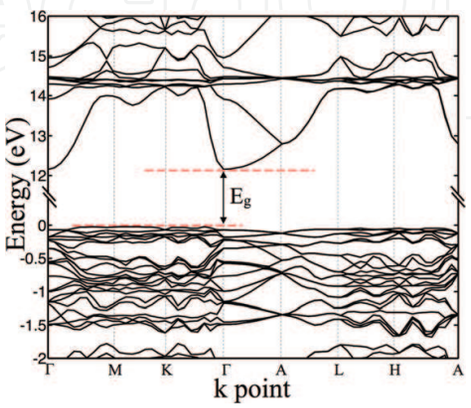

Figure 4. Simulated electronic band structure of LiCAF host crystal.

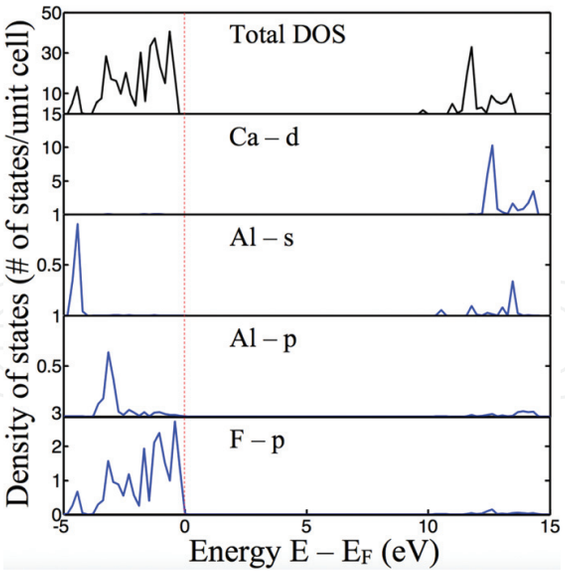

Figure 5. Total and projected density of states of LiCAF host.

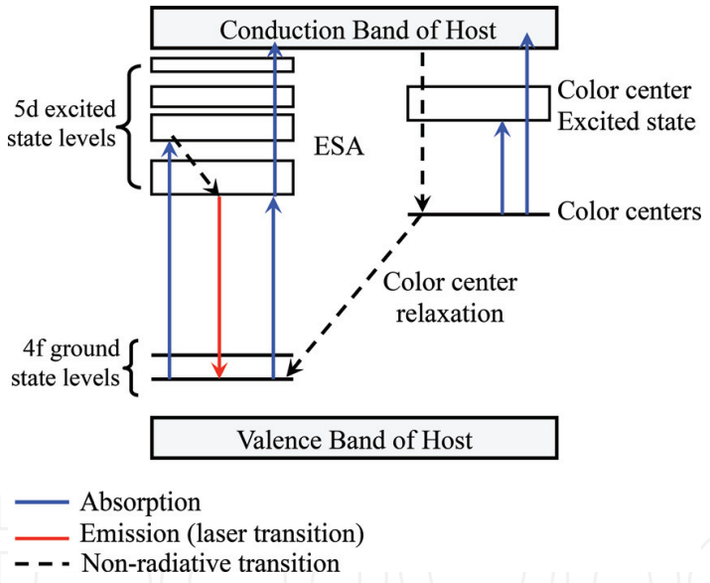

Figure 6. Excited state absorption (ESA) and color center formation in Ce^{3+}-doped fluoride gain media [27].

the LiCAF or LiSAF host tend to occupy the Ca^{2+} or Sr^{2+} octahedral sites [29]. The CeF_6 cluster in LiSAF will then have to compensate for the disparity in the size of the Ce^{3+} ion, which is 1.15 Å, and the Sr^{2+} ion, which is 1.27 Å. This compensation makes LiSAF prone to defects such as cracks and impurities during crystal growth [69]. For comparison, the size of the Ca^{2+} ion in LiCAF, which is 1.14 Å, is similar to that of the Ce^{3+} ion. Ce:LiCAF does not exhibit as much defects as Ce:LiSAF under the same growth conditions [69]. The larger amount of cracks and defect in Ce:LiSAF as well as the significant ESA as described above result to more pronounced solarization in this crystal. Both ESA and solarization compete with the lasing process and these results to lower laser conversion efficiency.

5. Numerical simulation of optimized resonator transients for generating ultrashort Ce:LiCAF laser pulses

Sub-nanosecond (0.7 ns), single-pulse, ~290 nm laser emission from a Ce:LiCAF crystal using an oscillator with a 25 mm cavity length and 25% output coupler reflection has been demonstrated experimentally. In this report, the end-pumping configuration was used to excite the crystal with an Nd:YAG laser emitting 266-nm wavelength (fourth harmonics), 5-ns pulses at 10 Hz repetition rate [70]. Another study reported the generation of 150-ps laser pulses from a 10-mm long Ce:LiCAF crystal. In this report, the laser oscillator was established using a cavity length of 15 mm, output coupler reflection of 30%, and 75 ps excitation pulses [71]. Despite the short pulse durations reported in these studies, the inherent properties of Ce:LiCAF provides the capability for this solid-state laser gain medium to generate even shorter UV pulse durations, which up to this point has not been fully realized. Numerical calculations play an important role in determining the influence of optical parameters, such as pumping energy, Q-value and cavity length on the output energy and pulse duration of a Ce:LiCAF UV laser, and hence in optimizing the laser oscillator design.

The Ce:LiCAF crystal used in the numerical calculations has 1 mol% Ce^{3+} ion doping and is 1 cm long. This crystal is placed inside a Fabry-Perot laser cavity of length L. It is end-pumped by the fourth harmonics (266 nm) of a ps Nd:YAG laser. The pump pulse is a Gaussian beam with 75 ps (FWHM) pulse duration. The end mirror of the laser cavity is flat with reflectivity denoted by R_1. The output coupler of the laser cavity is also flat with reflectivity denoted by R_2. It is assumed that both mirrors have uniform reflectivity within the emission bandwidth of the laser crystal. The optical properties of the Ce:LiCAF crystal given in **Table 2**, which is detailed in several papers, are used as calculation parameters [2, 20–22, 24–30].

Laser emission is approximated using a system of two homogeneous broadened singlet states. Eqs. (1)–(4) show the modified rate equations as it applies to multiple wavelengths, which accurately simulates the broad emission bandwidth of the Ce:LiCAF UV laser [72–74]:

$$\frac{\partial N_1}{\partial t} = P(t) + \left[\sum_1^n \sigma_{ai} I_i\right] N_o - \left[\sum_1^n \sigma_{ei} I_i + \frac{1}{\tau}\right] N_1 \tag{1}$$

$$P(t) = \frac{P_{in}\left[1 - \exp\left(-\alpha l\right)\right]\lambda_p}{hc\pi r^2 l} \exp\left[\frac{-4\ln\left(2\right)(t - t_o)^2}{\Delta t^2}\right] \tag{2}$$

$$\frac{\partial I_1}{\partial t} = \left[2(\sigma_{ei} N_1 - \sigma_{ai} N_0) l - \beta\right] \frac{I_i}{T} + A_i N_1 \tag{3}$$

$$T = \frac{2[L + l(n-1)]}{c} \tag{4}$$

The population density in the upper laser state as a function of time is given by Eq. (1) where N_0 is the lower-state population density, N_1 is the upper-state population density, $N = N_0 + N_1$ is the total doping density, I_i is the intensity of the laser with wavelength λ_i, τ is the fluorescence decay

Ce^{3+} doping concentration	1 mol%
Doping density, N	5×10^{17} cm^{-3}
Absorption coefficient at 266 nm (wavelength of pump laser)	4 cm^{-1}
Absorption cross-section, σ_{ai}	2.606×10^{-19} cm^{-2} at 290 nm
Emission cross-section, σ_{ei}	9.6×10^{-18} cm^{-2} at 290 nm
Refractive index, n	1.41
Fluorescence lifetime, τ	25 ns
Spontaneous emission constant, A_i	0.2×10^{-10} cm s^{-2}
Wavelength of pump laser, λ_p	266 nm
Radius of pump beam inside the crystal	100 μm
Pulse duration of pump pulse	75 ps
Planck's constant, h	$6.62606957 \times 10^{-34}$ J s
Speed of light, c	3×10^{8} m s^{-2}
Reflectivity of end mirror, R_1	100%

Table 2. Optical properties of the Ce:LiCAF crystal and values of parameters that were kept constant in numerical simulations.

time. P is the rate of pumping which is further described by Eq. (2) where λ_p is the pump laser's wavelength, P_{in} is the power of the pump, l is the Ce:LiCAF crystal's length, r is the pump beam's radius inside the laser medium, h is Planck's constant which is $6.62606957 \times 10^{-34}$ J s, c is the speed of light which is 3×10^{8} m s^{-1}, α is the absorption coefficient of Ce:LiCAF at 266 nm (pump laser's wavelength), t is the duration of pumping, Δt is the laser pump's pulse duration, and t_o is the time when P_{in} is maximum. P has a unit of s^{-1}. The laser intensity inside the cavity as a function of time is given by Eq. (3) where β is the round-trip loss defined by $\beta = -\ln(R_1R_2)$ in which case R_1 is the end mirror's reflectivity and R_2 is the output coupler's reflectivity, σ_{ei} is the emission cross-section at wavelength λ_i, σ_{ai} is the absorption cross-section at wavelength λ_i [24], A_i is a constant that simulates spontaneous emission at wavelength λ_i and its value is considered equal for all wavelengths since the duration of pumping is much greater than the memory time of the system of equations [72–74]. In this work, the value of A_i is about three times longer than the decay time of fluorescent dyes as estimated using the fluorescence decay time of Ce:LiCAF, which us about 25 ns. T is the cavity round-trip time as defined by Eq. (4) where L is the laser cavity's length and n is the Ce:LiCAF crystal's refractive index. The values of the constants used in the simulations are given in **Table 2**.

Rate Eqs. (1)–(4) were used to model the experimental results [71, 75] by using the same parameters that were used in the experiment [71]. The Ce:LiCAF crystal length, l = 10 mm; $N = 5 \times 10^{17}$ cm^{-3} for a doping concentration of 1 mol%; refractive index, n = 1.41; length of cavity, L = 15 mm; reflectivity of end mirror, R_1 = 100%; reflectivity of output coupler, R_2 = 30%; radius of pump beam, r = 100 μm; energy of pump, E_{pump} = 94 μJ; and the laser pump's pulse duration, Δt = 75 ps. These values are given in **Tables 2** and **3**. The spectro-temporal plot of the simulated broadband emission from 286 to 290 nm is shown in **Figure 7**. The corresponding

spectral dynamics derived from integrating along the horizontal axis of **Figure 7** is shown in **Figure 8**. The maximum laser intensity is observed at around 288.5 nm. This corresponds to the wavelength where the gain coefficient is also maximum. The distinct feature observed at around 289.5 nm is consistent with experimental observation [20–30] and is reported to be present for

Crystal length, l	10 mm
Cavity length, L	15 mm
Reflectivity of output coupler, R_2	30%
Energy of pump beam	94 μJ

Table 3. Ce:LiCAF resonator parameters used to reproduce experimental results.

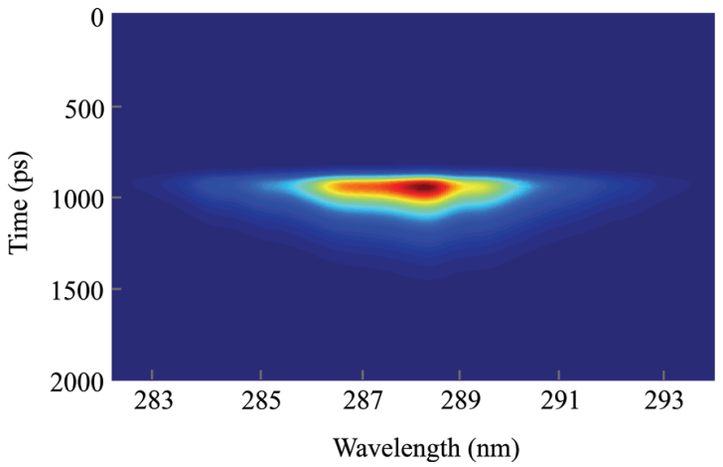

Figure 7. Spectro-temporal evolution of the low-Q, short cavity Ce:LiCAF laser pulse emission obtained numerically using the rate equations. The oscillator parameters are $N = 5 \times 10^{17}$ cm^{-3}, $l = 10$ mm, $L = 15$ mm, $R_1 = 100\%$, $R_2 = 30\%$, $r = 100$ μm, $\Delta t = 75$ ps, $E_{\text{pump}} = 94$ μJ, and $n = 1.41$.

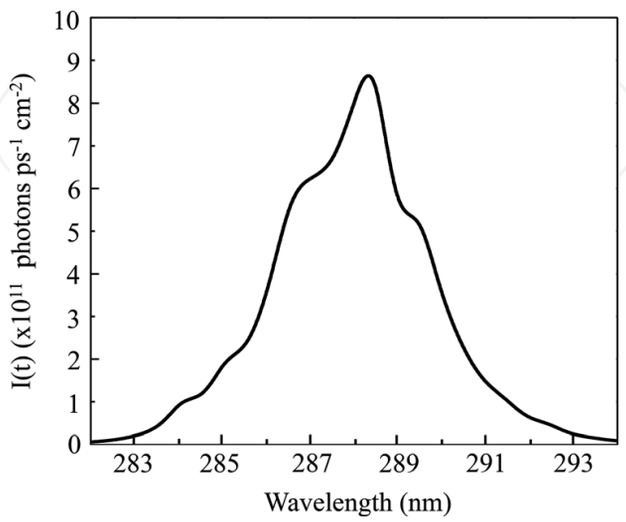

Figure 8. Spectral dynamics of the numerically calculated spectro-temporal profile in **Figure 7**.

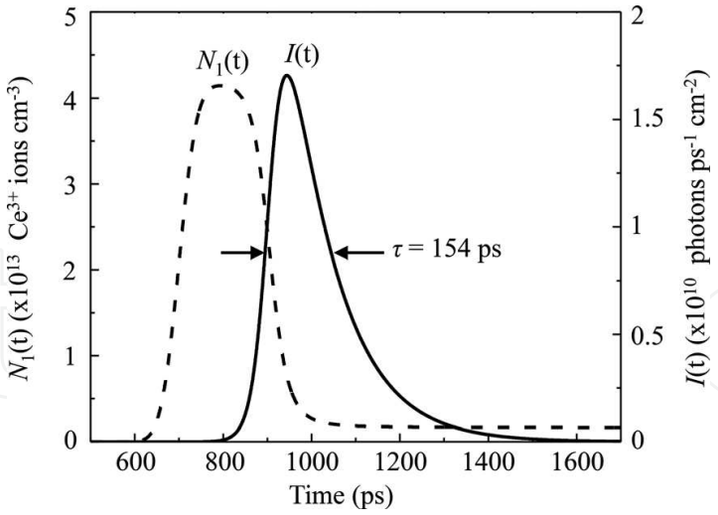

Figure 9. Temporal dynamics of the numerically calculated spectro-temporal profile in **Figure 7**.

any amount of doping. **Figure 9** shows the temporal dynamics of the laser emission, which was derived by integrating along the vertical axis of **Figure 7**. Electron density builds up in the upper laser state of Ce:LiCAF until population inversion is achieved. Lasing threshold is reached around 0.3 ns after the onset of the pump pulse (not shown). The lasing threshold was measured when laser emission is observed. Peak emission is achieved about 0.5 ns after the onset of the pump pulse. The pulse duration is estimated from the full-width-at-half-maximum (FWHM) to be around 154 ps. Results of the temporal dynamics simulation are comparable, within the limits of jitter, to experimental results estimated from the streak camera image that was obtained experimentally [71, 75]. The experimental pulse duration is about 150 ps [71]. The good agreement between the numerical and experimental results indicate that the system of two homogeneous broadened singlet states and the modified rate equations as it applies to multiple wavelengths provide good approximations for predicting the experimental outcome. In succeeding calculations, the model described above was then used to optimize the optical parameters in order to achieve ultrashort pulse emission from a Ce:LiCAF solid-state UV laser.

Eqs. (1) and (2) clearly show that the rate of change of excited state population density and laser intensity strongly depend on the pump energy. Therefore, we solved the rate equations for varying pump energies from 25 to 600 μJ in order to determine its effect on the temporal evolution of the Ce:LiCAF laser emission. Results are shown in **Figure 10a–f**. The parameters used in the numerical simulation were kept constant except for the pump energy. These parameters were the same as the experimental parameters, i.e. crystal length, l = 10 mm; $N = 5 \times 10^{17}$ cm^{-3} for 1 mol% doping concentration; cavity length, L = 15 mm; end mirror reflectivity, R_1 = 100%; output coupler reflectivity, R_2 = 30%; pump beam radius, r = 100 μm; and pulse duration of the laser pump, Δt = 75 ps. Lasing is achieved when the pump energy is around 37.5 μJ (**Figure 10b**). **Figure 10c–f** clearly shows that the laser pulse duration shortens as the pump energy is increased up to 360 μJ (**Figure 10d**). As the pump energy is increased, the time delay between the onset of laser emission and the pump also decreases due to the earlier occurrence of population inversion. The laser emission at different pump energies (**Figure 11**) shows that the spectral bandwidth becomes broader when the

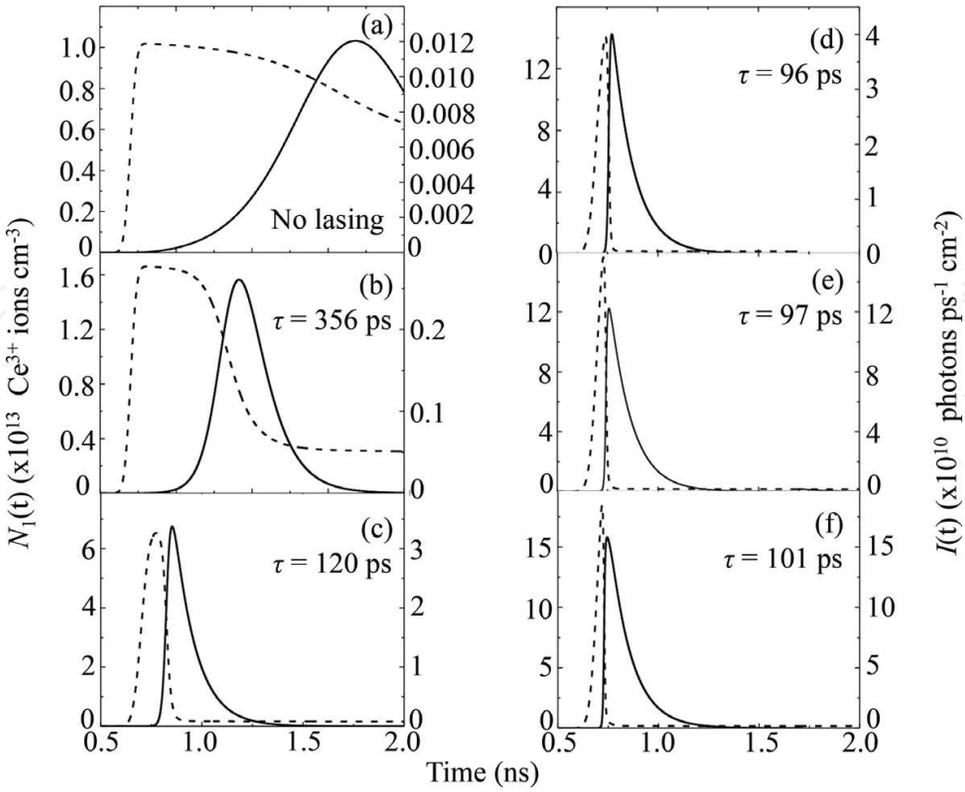

Figure 10. Temporal evolution of the Ce:LiCAF laser emission for different pump energies: (a) 25 μJ, (b) 37.5 μJ, (c) 150 μJ, (d) 360 μJ, (e) 450 μJ, and (f) 600 μJ. The dashed plot represents $N_1(t)$ while the solid plot represents $I(t)$. The following parameters were kept constant: $N = 5 \times 10^{17}$ cm^{-3}, $l = 10$ mm, $L = 15$ mm, $R_1 = 100\%$, $R_2 = 30\%$, $r = 100$ μm, $\Delta t = 75$ ps, and $n = 1.41$.

pump energy is increased. This is expected since wavelengths close to 288 nm have sufficient energy to achieve considerable gain.

The laser output energy was calculated using

$$E_{out} = \int_0^t \int_{\lambda_1}^{\lambda_n} \frac{(1 - R_2)\pi r^2 hc}{\lambda} I(\lambda, t) \tag{5}$$

where $I(\lambda, t)$ is the laser intensity at wavelength λ and time t. As expected, the output energy increases as the pump energy is increased. This trend is shown in **Figure 12**.

Figures 10 and **12** indicate that in theory, increasing the pump energy would result to an ultrashort (ps pulse duration) laser pulse with micro Joule energy. However, absorption saturation and the damage threshold of the crystal limit the choice of pump energy in experiments. Eq. (4) is therefore integrated in order to determine where absorption saturation of the 266-nm pump begins for the crystal used in experiments. The crystal is 1-cm long and the total number of Ce^{3+} ions is 6.3×10^{14}. The absorption saturation is determined to begin at 1.4 mJ pump energy when the beam spot radius is 100-μm. However, the damage threshold of Ce:LiCAF at 266 nm (wavelength of pump) is about 2 J/cm^2 [76]. Therefore, the maximum pump energy

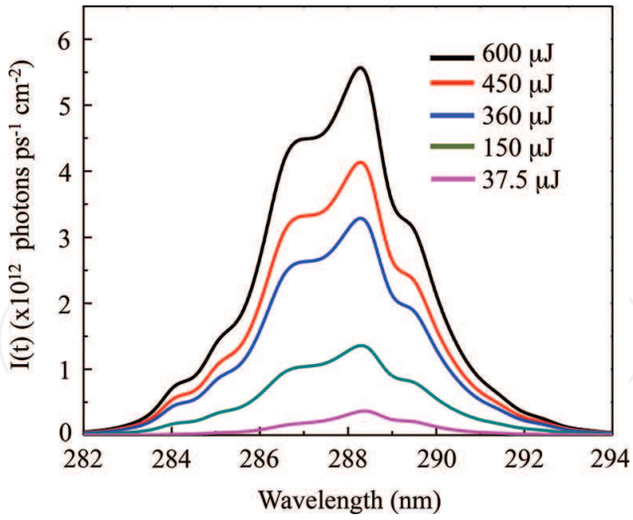

Figure 11. Spectral profiles of the laser emissions for the different pump energies shown in **Figure 10**.

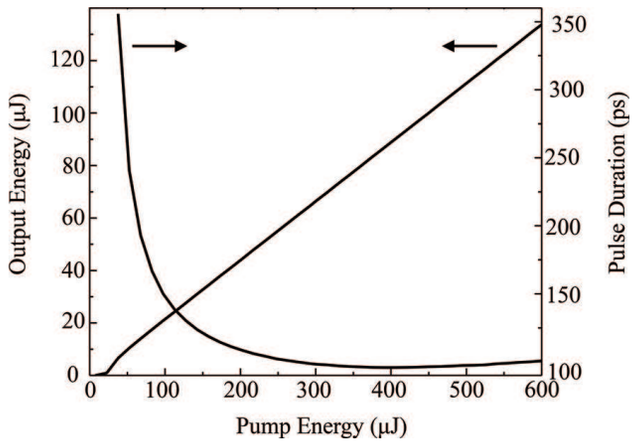

Figure 12. Output energy and pulse duration for different pump energies. Calculation parameters used simulate experimental conditions: $N = 5 \times 10^{17}$ cm^{-3}, $l = 10$ mm, $L = 15$ mm, $R_1 = 100\%$, $R_2 = 30\%$, $r = 100$ μm, $\Delta t = 75$ ps, and $n = 1.41$. The slope efficiency is about 23%.

used in the simulations is 600 μJ as the damage threshold is reached at this amount of energy for a 100 μm-beam radius. The laser cavity that was used in Ref. [71] amounts to a laser emission efficiency of about 23% as indicated by **Figure 12**. The same figure (**Figure 12**) also shows that a 360 μJ—pump energy could generate 96 ps pulses. This would be the shortest pulse duration. From this observation, the spectro-temporal evolution of the laser pulse emission at 360 μJ—pump energy is calculated and shown in **Figure 13**.

On the other hand, the suppression of the laser emission is evident where the Ce:LiCAF's gain coefficient is lower, particularly on either side of the 288.5-nm wavelength. Because of this, the maximum intensity of the broadband UV laser emission is expected at about 288.5 nm. **Figure 14** confirms that the gain coefficient is still maximum at around 288.5 nm and hence, a shift in the position of the laser peak is not expected. **Figure 10d** shows the temporal evolution of the laser pulse from 284 to 293 nm. This wavelength range spans the whole bandwidth of the UV laser

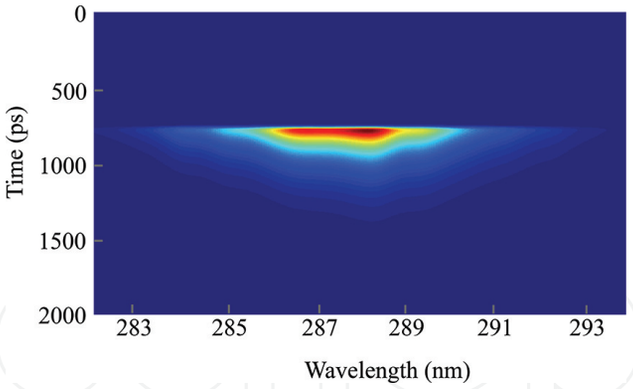

Figure 13. Spectro-temporal evolution of the shortest possible laser pulse duration (96 ps) achievable using experimental resonator parameters $N = 5 \times 10^{17}$ cm^{-3}, $l = 10$ mm, $L = 15$ mm, $R_1 = 100\%$, $R_2 = 30\%$, $r = 100$ μm, $\Delta t = 75$ ps, $n = 1.41$, and 360-μJ pump energy.

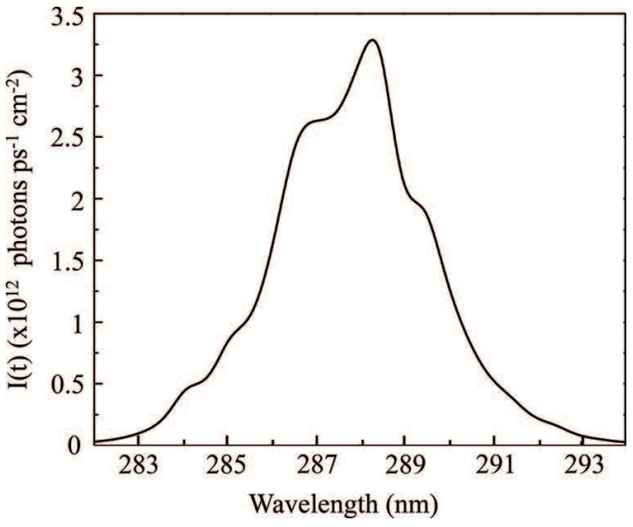

Figure 14. Spectral dynamics of the shortest achievable laser pulse duration (96 ps). The corresponding temporal dynamics is shown in **Figure 10d**.

emission from Ce:LiCAF. By measuring the full width at half maximum (FWHM), the duration of the laser pulse is estimated to be about 96 ps. These calculations indicate that the shortest pulse duration that can be achieved without damaging the crystal is around 96 ps with a slope efficiency of around 23% assuming that the same parameters for the laser cavity and gain medium from the experiment of reference [71] are used.

The design of the laser oscillator cavity is important for optimizing laser emission especially for solid-state gain media. The cavity transient method, which uses the relationship between the cavity round trip time and the fluorescence decay time of the laser gain medium offers a simplified means of generating short laser pulses directly from a cavity that is optically pumped [34, 35]. With this method, factors such as the cavity lifetime of the photon, energy of the pump, and duration of the laser pump pulse strongly influences the pulse duration of laser emission. Moreover, the cavity lifetime of the photon (τ_c) which is described by Eq. (6) is determined by the length of the cavity and the reflectivity of the mirrors.

$$\tau_c = \frac{L + n(l-1)}{c(1 - \ln(R_1 R_2))} \tag{6}$$

The photon cavity lifetime (τ_c) decreases as the cavity length, L, or the mirror reflectivities, R_1 and R_2, decrease. Short-pulse laser emission in solid-state gain media can be achieved through the combination of a photon cavity lifetime (τ_c) that is smaller compared to the duration of the pump laser pulse and moderate resonator transients. The latter is brought about by the interaction between the photons in the cavity and the excess population inversion. Previous works have reported using resonator transients in dye lasers to obtain laser pulse durations that are an order of magnitude shorter than the pulse duration of the pump laser [34–36].

In order to extend the technique of resonator transients to solid-state gain media, the rate equations were solved for a variety of output coupler reflectivities and cavity lengths. The optimum condition for setting up a transient cavity was first determined by using a constant value for the output coupler reflectivity while varying the cavity lengths from L = 2 mm to L = 10 mm. The following summarizes the values of the parameters that were kept constant: R_1 = 100%, R_2 = 30%, l = 1 mm, r = 100 μm, pumping energy = 140 μJ, and Δt = 75 ps. The total number of Ce^{3+} ions in the crystal considered here is 6.3×10^{13}. By integrating Eq. (4), the absorption saturation of the 266 nm pump begins at pump energy of 142.8 μJ. Therefore, the maximum energy used in all calculations involving this 1-mm crystal, including **Figures 15–18**, is 140 μJ. Note that the 30% output coupler reflectivity is the same as what was used in the experiment of reference [71]. Calculations show that shorter pulse durations are obtained when the cavity length is shortened. These results are presented in **Figure 15a–d**. It should be noted

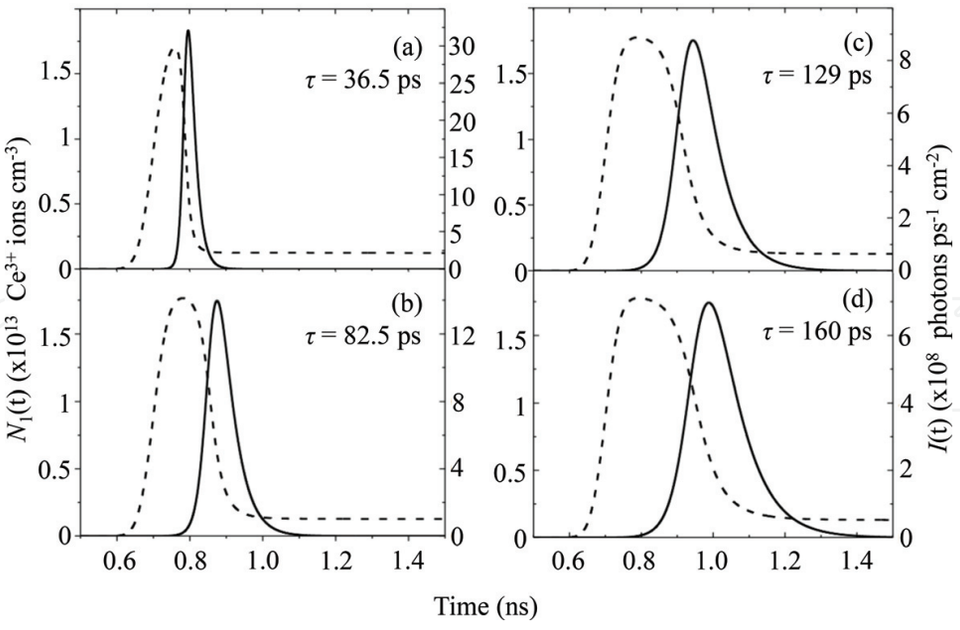

Figure 15. Temporal evolution of the Ce:LiCAF laser emission for different cavity lengths, L, of (a) 2 mm (b) 5 mm, (c) 8 mm, and (d) 10 mm. $I(t)$ is represented by the solid plot while $N_1(t)$ is represented by the dashed plot. The values of the following parameters that were kept constant are: $N = 5 \times 10^{17}$ cm^{-3}, l = 1 mm, R_1 = 100%, R_2 = 30%, r = 100 μm, Δt = 75 ps, n = 1.41, and pump energy = 140 μJ. The pump energy was chosen based on the effect of pump energy on pulse duration shown in **Figure 16**.

that the calculation model does not consider energy loss due to cavity length and therefore, the numerical results could over estimate experimental results particularly when the cavity length is long. Regardless of the over estimation, the numerical results show that it is favorable to have a shorter cavity length in order to achieve a shorter pulse durations As Eq. (5) predicts, smaller photon cavity lifetimes are obtained from smaller cavity lengths and as a consequence, shorter laser pulse durations are also obtained. However, the length of the crystal, *l*, dictates the limit on the practical size of the cavity, although it would appear from Eq. (5) that ultrashort pulses could be obtained by using ultrashort cavity lengths. From the point of view of crystal growth, 1 mm is a practical crystal length for a LiCAF crystal doped with 1 mol% Ce^{3+}, and for fluoride crystals with 1 mol% rare earth doping in general. A 140-μJ pump energy was used based on **Figure 16**, which shows how the pump energy affects the pulse duration. The output energy is about the

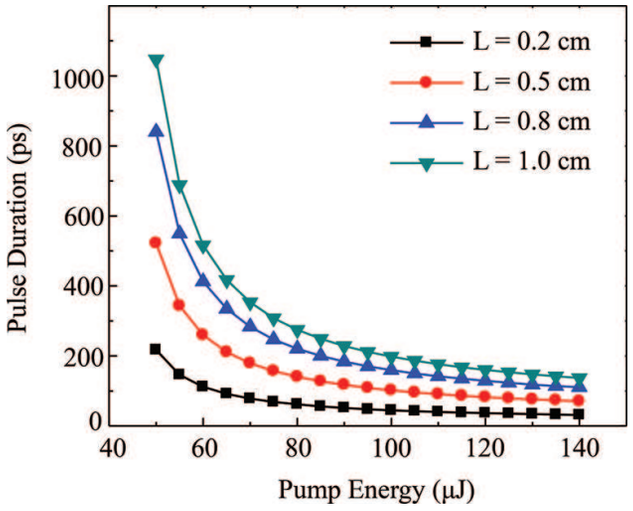

Figure 16. Effect of pump energy on the pulse duration of the Ce:LiCAF laser emission.

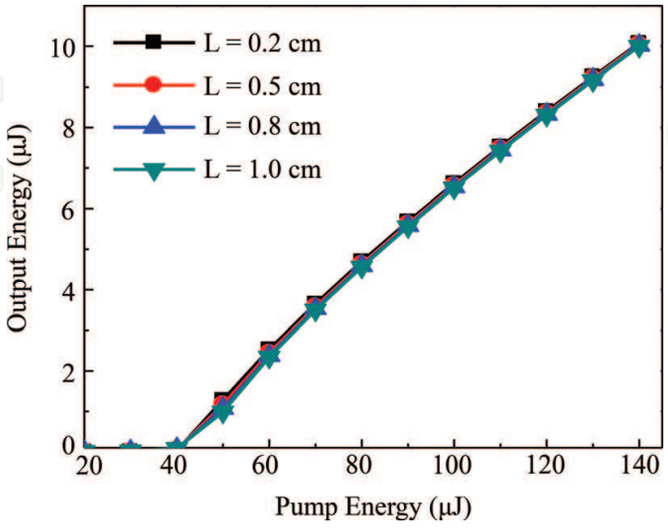

Figure 17. Output energy for the different cavity lengths considered.

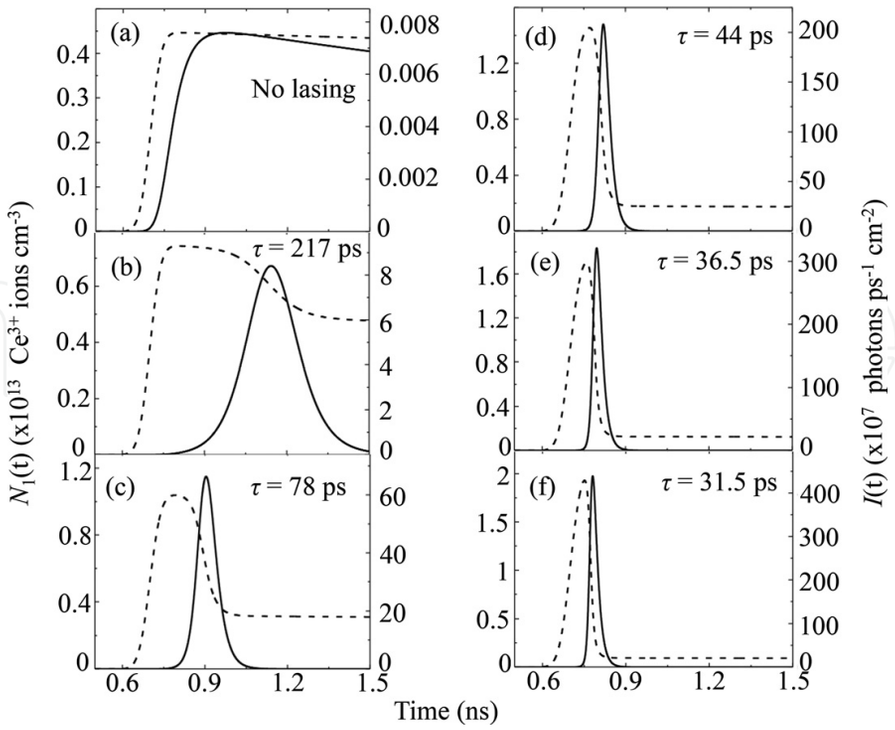

Figure 18. Temporal profile of the laser pulse for different pump energies using a $L = 2$ mm laser oscillator (short cavity). The energies used are: (a) 30 μJ, (b) 50 μJ, (c) 70 μJ, (d) 100 μJ, (e) 120 μJ and (f) 140 μJ. $I(t)$ is represented by the solid plot while $N_1(t)$ is represented by the dashed plot. The values of the following parameters that were kept constant are: $N = 5 \times 10^{17}$ cm^{-3}, $l = 1$ mm, $R_1 = 100\%$, $R_2 = 30\%$, $r = 100$ μm, $\Delta t = 75$ ps, and $n = 1.41$. **Figure 19** summarizes the laser output energy and pulse duration for the energies used in **Figure 18**. A duration of 31.5 ps is the shortest pulse duration that can be obtained for $L = 2$ mm and $l = 1$ mm (short resonator cavity). The damage threshold and the absorption saturation of the crystal limit this pulse duration. Therefore, optimizing growth conditions and doping levels can achieve shorter pulse durations. Nevertheless, this is much shorter than the pulse duration that can be obtained using the same values for the pump energy (140-μJ), and output coupler reflectivity (30%), but with a cavity length of $L = 15$ mm and a crystal length of $l = 10$ mm. As **Figure 12** shows, this laser oscillator that is longer produces pulse duration of 123 ps. On the other hand, a lower output energy is obtained for the same pump energy when the length of the crystal and hence the length of the cavity are shortened. For instance, about 10 μJ output energy is obtained using $L = 2$ mm and $l = 1$ mm whereas about 30 μJ output energy is obtained using $L = 15$ mm and $l = 10$ mm for the same 140 μJ pump energy.

same for the cavity lengths considered ($L = 2$–10 mm) as shown in **Figure 17**. The slope efficiency is about 10%.

Figure 18a–f shows the temporal evolution of the laser pulse from a short cavity ($L = 2$ mm) for various pump energies. The same crystal and laser cavity parameters used in simulating **Figure 15a–d** were used in **Figure 18a–f**. A single laser pulse with ps pulse duration is achieved when the energy of the pump laser is varied from 50 μJ to 140 μJ, with a 31.5 ps pulse duration obtained at 140 μJ. Even though it is not shown in the figure, it is worth noting that when the energy of the pump is greater than 3 mJ, lasing occurs almost immediately. This pump energy leads to excess population inversion, as it is much higher than the lasing threshold. As a result of the interaction between the excess population inversion and the photons in the cavity, resonator transients are formed and these are manifested as damped relaxation oscillation or spiking in the laser pulse profile. The laser pulse will eventually approach the shape of the pump pulse when the energy of the pump is increased further,

although the resonator transients (spikes) will still be visible. These spikes have not been observed experimentally since the pump energy in experiments is not high enough.

As discussed earlier, the pump energy and pulse duration of the laser pump as well as the photon cavity lifetime which is determined by the length of the oscillator cavity and the reflectivity of the mirrors strongly influences the pulse duration of the resulting laser emission. Therefore, numerical simulations are performed to quantify the effect of the reflectivity of the output coupler on the laser pulse duration for various pump energies. The results are shown in **Figure 20**. Other parameters are kept constant as follows: $N = 5 \times 10^{17}$ cm^{-3}, $L = 2$ mm, $l = 1$ mm, $R_1 = 100\%$, $r = 100$ μm, and $\Delta t = 75$ ps. It can be observed that a low-Q cavity results to a short laser pulse. The shortest pulse duration is about 31.5 ps when the output coupler

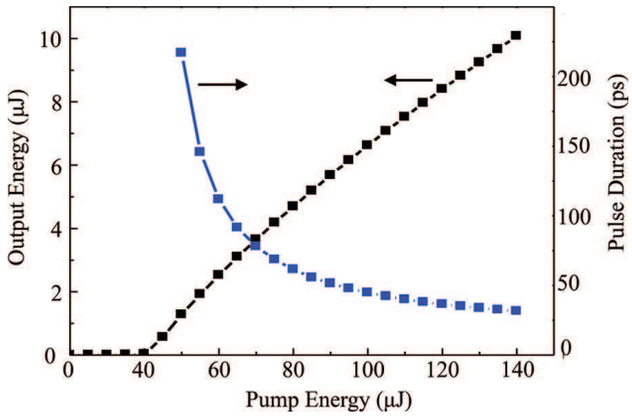

Figure 19. Output energy and pulse duration of the laser pulse from a short cavity oscillator ($L = 2$ mm) for different pump energies. The following parameters were kept constant: $N = 5 \times 10^{17}$ cm^{-3}, $l = 1$ mm, $R_1 = 100\%$, $R_2 = 30\%$, $r = 100$ μm, $\Delta t = 75$ ps, and $n = 1.41$. The slope efficiency is about 24%.

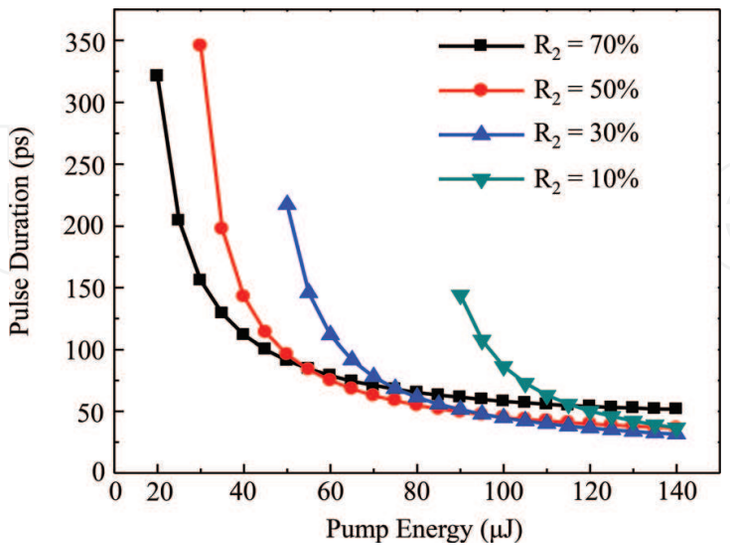

Figure 20. Dependence of pulse duration on pump energy for different output coupler reflectivities: 10, 30, 50, and 70%. A short cavity oscillator ($L = 2$ mm) was assumed and the other parameters were kept constant as follows: $N = 5 \times 10^{17}$ cm^{-3}, $l = 1$ mm, $R_1 = 100\%$, $r = 100$ μm, $\Delta t = 75$ ps, and $n = 1.41$.

reflectivity is 30%. Taking a closer look at the temporal dynamics of the laser pulse for various output coupler reflectivity (**Figure 21a–d**) shows that the threshold for laser emission is reached earlier when the reflectivity is increased. As a result, the laser pulse duration will be longer when the output coupler is highly reflecting. Consequently, a low-Q laser resonator that is established using an output coupler with low reflectivity is required in order to generate short laser pulses low-Q cavity is therefore desirable for generating short-pulse laser emission. **Figure 21a–d** was simulated using laser pump energy of 140 μJ. The choice of pump energy is

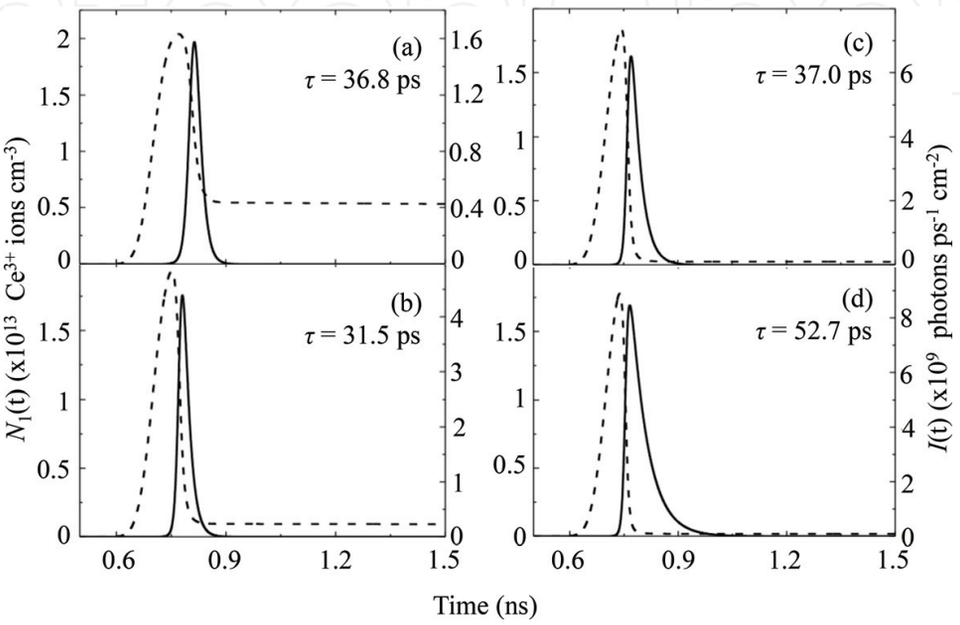

Figure 21. Temporal evolution of the laser emission for various output coupler reflectivity (R_2). The length of the short Ce: LiCAF cavity oscillator is L = 2 mm. The various R_2 values considered are: (a) 10%, (b) 30%, (c) 50%, and (d) 70%. The following parameters were kept constant: $N = 5 \times 10^{17}$ cm^{-3}, l = 1 mm, R_1 = 100%, Δt = 75 ps, r = 100 μm, n = 1.41, and pumping energy is 140 μJ. The pump energy was chosen based on results in **Figures 19** and **20**. Solid graph represents $I(t)$ while dashed graph represents $N_1(t)$.

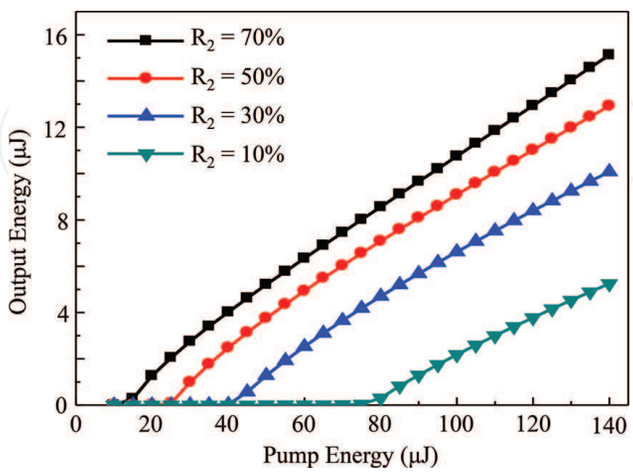

Figure 22. Output energy as a function of pump energy for different output coupler reflectivities ranging from 10 to 70%. A short cavity oscillator (L = 2 mm) was assumed and the other parameters were kept constant as follows: $N = 5 \times 10^{17}$ cm^{-3}, l = 1 mm, R_1 = 100%, r = 100 μm, Δt = 75 ps, and n = 1.41.

based on the results shown in **Figures 19** and **20**, where pulse duration decreases with increasing energy within the limits of absorption saturation. Theoretically, shorter pulse durations can be achieved using an output coupler with less than 10% reflectivity. Practically, the threshold energy and the slope efficiency limit the choice of reflectivity. As **Figure 22** shows, higher pump energies are needed to achieve lasing in a low-Q laser resonator. If the reflectivity of the output coupler is 10%, for instance, the lasing threshold for obtaining a 31.5-ps laser pulse is 80 μJ and the slope efficiency is 8%. However, increasing the output coupler reflectivity to 30% decreases the threshold energy to 40 μJ and increases the slope efficiency to 10%.

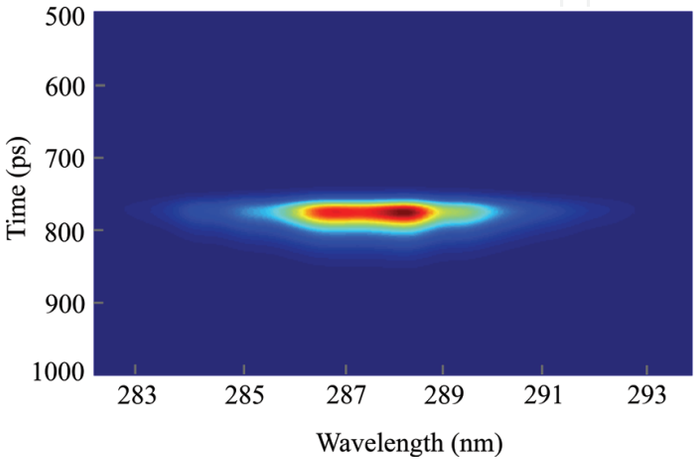

Figure 23. Spectro-temporal evolution of the broadband, short-pulse Ce:LiCAF laser emission from an optimized low-Q (R_2 = 30%), short cavity (L = 2 mm) oscillator. A short laser pulse with about 31.5-ps pulse duration, broadband emission centered at 288.5-nm wavelength, and 10 μJ output energy can be obtained practically from a 1-mm long, 1 mol% Ce^{3+}-doped LiCAF crystal when pumped by a 266-nm, 75-ps pump pulse with 140 μJ pump energy. A slope efficiency of about 10% is also feasible with pump energies that are far from the crystal's absorption saturation and damage threshold.

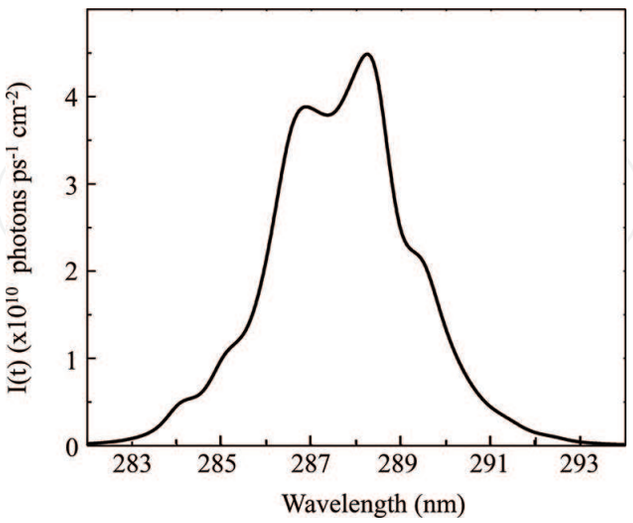

Figure 24. Spectral profile of the broadband, short-pulse Ce:LiCAF laser emission from an optimized low-Q (R_2 = 30%), short cavity (L = 2 mm) oscillator. Temporal dynamics is shown in **Figure 21b**.

According to **Figures 19–22**, the optimal transient cavity laser resonator has a 2-mm long cavity and a 30% output coupler reflectivity. These figures also indicate that about 31.5-ps laser pulse duration and about 10% slope efficiency is possible when a 1 mol% Ce-doped LiCAF crystal that is 1 mm long is excited by a 266-nm wavelength pump laser with 75-ps pulse duration and 140 μJ pump energy. These conditions already take into account the crystal's damage threshold, which is about 600-μJ of pump energy for a 100-μm-beam radius as well as its absorption saturation, which is about 142.8 μJ. The 31.5-ps pulse duration is significantly shorter than the experimental pulse duration obtained by reference [71]. The spectro-temporal and the spectral profiles of the broadband 31.5-ps laser pulse are shown in **Figures 23** and **24**, respectively. The spectral profile is consistent with the trend observed in **Figure 11**, regardless of resonator cavity parameters. Maximum gain coefficient is also achieved at around 188.5 nm.

6. Conclusion

In summary, the transient cavity method is extended to a solid-state gain medium. Numerical simulations show that the same principles used to generate ultrashort laser pulses in dye lasers using this technique can be applied to solid-state gain media to generate ultrashort broadband pulses in the UV region. The laser gain medium was represented as a system of two homogeneous broadened singlet states and the numerical simulations solved the laser rate equations for broadband emission. The spectral and temporal evolution of the resulting laser emission was investigated in order to find the optimal cavity length and output coupler reflectivity that will give rise to the formation of resonator transients in the laser oscillator cavity. The calculations reveal that a laser oscillator with a short cavity and a low Q is ideal for the formation of resonator transients, which then lead to ultrashort (ps) laser emission. Specifically, a 2-mm cavity length and a 10% output coupler reflectivity can be used to generate a single 31.5 ps pulse using a 1-mm long Ce:LiCAF crystal with 1 mol% Ce^{3+} ion doping concentration. Although this work used Ce:LiCAF crystal as the laser gain medium, the transient cavity method can also be applied to generate ultrashort laser pulses using other rare earth-doped fluoride crystals.

Acknowledgements

This research was supported by the Massey University Research Fund 2018 (MURF 2018 Project No. 1000020752), Institute of Laser Engineering, Osaka University Collaborative Research Grant (Grant no. 2017B1-RADUBAN), JSPS-VAST Joint Research Project (2011–2014), the Vietnam National Foundation for Science and Technology Development (NAFOSTED) under Grant Numbers 103.06.89.09 and 103.03-2015.29. M. Cadatal-Raduban and M.V. Luong are very grateful to K.G. Steenbergen and P. Schwerdtfeger for their input and valuable discussions on the numerical simulation of the electronic properties of the LiCAF and LiSAF host.

Author details

Marilou Cadatal-Raduban[1]*, Minh Hong Pham[2], Luong Viet Mui[3], Nguyen Dai Hung[2] and Nobuhiko Sarukura[3]

*Address all correspondence to: m.raduban@massey.ac.nz

1 Centre for Theoretical Chemistry and Physics, Institute of Natural and Mathematical Sciences, Massey University, Auckland, New Zealand

2 Institute of Physics, Vietnam Academy of Sciences, Hanoi, Vietnam

3 Institute of Laser Engineering, Osaka University, Suita, Osaka, Japan

References

[1] Link S, Durr HA, Eberhardt W. Femtosecond spectroscopy. Journal of Physics: Condensed Matter. 2001;**13**:7873-7884. PII: S0953-8984(01)26618-1

[2] Sarukura N, Liu Z, Ohtake H, Segawa Y, Dubinskii MA, Semashko VV, Naumov AK, Korableva SL, Abdulsabirov RY. Ultraviolet short pulses from an all-solid-state Ce:LiCAF master-oscillator power-amplifier system. Optics Letters. 1997;**22**:994-996. DOI: 10.1364/OL.22.000994

[3] Assion A, Baumert T, Bergt M, Brixner T, Kiefer B, Seyfried V, Strehle M, Gerber G. Control of chemical reactions by feedback-optimized phase-shaped femtosecond laser pulses. Science. 1998;**282**:919-922. DOI: 10.1126/science.282.5390.919

[4] Baltuška A, Udem T, Uiberacker M, Hentschel M, Goulielmakis E, Gohle C, Holzwarth R, Yakovlev VS, Scrinzi A, Hänsch TW, Krausz F. Attosecond control of electronic processes by intense light fields. Nature. 2003;**421**:611-615. DOI: 10.1038/nature01414

[5] Nam KB, Li J, Kim KH, Lin JY, Jiang HX. Growth and deep ultraviolet picosecond time-resolved photoluminescence studies of AlN/GaN multiple quantum wells. Applied Physics Letters. 2001;**78**:3690-3692. DOI: 10.1063/1.1377317

[6] Miyamoto I, Horn A, Gottmann J. Local melting of glass material and its application to direct fusion welding by Ps-laser pulses. Journal of Laser Micro/Nanoengineering. 2007;**2**: 7-14. DOI: 10.2961/jlmn.2007.01.0002

[7] Pissadakis S, Konstantaki M. Photosensitivity of germanosilicate fibers using 213 nm, picosecond Nd:YAG radiation. Optics Express. 2005;**13**:2605-2610. DOI: 10.1364/OPEX.13.002605

[8] Chen Y, Vertes A. Adjustable fragmentation in laser desorption/ionization from laser-induced silicon microcolumn arrays. Analytical Chemistry. 2006;**78**:5835-5844. DOI: 10.1021/ac060405n

[9] Raciukaitis G, Jacinavicius A, Brikas M, Balickas S. "Picosecond lasers in micromachining," Proceedings of ICALEO, Laser Microfabrication Conference, 2003, p. M308. http://lia.scitation.org/doi/10.2351/1.2164480

[10] Weickhard C, Tonnies K. Short pulse laser mass spectrometry of nitrotoluen: Ionization and fragmentation behavior. Rapid Communications in Mass Spectrometry. 2002;**16**:442-446. DOI: 10.1002/rcm.567

[11] Roy S, Meyer TR, Gord JR. Time-resolved dynamics of resonant and nonresonant broadband picosecond coherent anti-Stokes Raman scattering signals. Applied Physics Letters. 2005;**87**:264103. DOI: 10.1063/1.2159576

[12] Gedvilas M, Raciukaitis G. Investigation of UV picosecond laser ablation of polymers. In: Proc. SPIE 6157, Workshop on Laser Applications in Europe. 2005. p. 61570T. DOI: 10.1117/12.661141

[13] Wintner E. Numerical evaluation of optical pumpprobe experiments. Journal of Applied Physics. 1985;**57**:1533-1537. DOI: 10.1063/1.334467

[14] Watanabe S, Endoh A, Watanabe M, Sarukura N, Hata K. Multiterawatt excimer-laser system. Journal of the Optical Society of America B-Optical Physics. 1989;**6**:1870-1876. DOI: 10.1364/JOSAB.6.001870

[15] Watanabe S, Endoh A, Watanabe M, Surakura N. Single-shot measurement of subpicosecond KrF pulse width by three-photon fluorescence of the XeF visible transition. Optics Letters. 1988;**13**:996-998. DOI: 10.1364/OL.13.000996

[16] Ehrlich DJ, Moulton PF, Osgood RM Jr. Ultraviolet solid-state Ce:YLF laser at 325 nm. Optics Letters. 1979;**4**:184-186. DOI: 10.1364/OL.4.000184

[17] Ehrlich DJ, Moulton PF, Osgood RM Jr. Optically pumped Ce:LaF_3 laser at 286 nm. Optics Letters. 1980;**5**:339-341. DOI: 10.1364/OL.5.000339

[18] Dubinskii MA, Abdulsabirov RY, Korableva SL, Naumov AK, Semashko VV. 18th International Quantum Electronics Conference, OSA Technical Digest. Vol. 548. Washington, DC: Optical Society of America; 1992

[19] Dubinskii MA, Abdulsabirov RY, Korableva SL, Naumov AK, Semashko VV. A new active medium for a tunable solid-state UV laser with an excimer pump. Laser Physics. 1994;**4**:480

[20] Dubinskii MA, Semashko VV, Naumov AK, Abdulsabirov RY, Korableva SL. Active medium for all solid-state tunable W laser. OSA Proceedings Advanced Solid-State Lasers. 1993;**15**:195-198. DOI: 10.1364/ASSL.1993.LM5

[21] Dubinskii MA, Semashko VV, Naumov AK, Abdulsabirov RY, Korableva SL. Spectroscopy of a new active medium of a solid-state UV laser with broadband single-pass gain. Laser Physics. 1993;**3**:216-217

[22] Dubinskii MA, Semashko VV, Naumov AK, Abdulsabirov RY, Korableva SL. Ce^{3+}-doped colquiriite—A new concept of all-solid-state tunable ultraviolet laser. Journal of Modern Optics. 1993;**40**:1-5. DOI: 10.1080/09500349314550011

[23] Marshall CD, Speth JA, Payne SA, Krupke WF, Quarles GJ, Castillo V, Chai BHT. Ultraviolet laser emission properties of Ce^{3+}-doped LiSrAlF6 and LiCaAlF6. Journal of the Optical Society of America B. 1994;**11**:2054-2065. DOI: 10.1364/JOSAB.11.002054

[24] Liu Z, Kozeki T, Suzuki Y, Sarukura N. Chirped-pulse amplification of ultraviolet femtosecond pulses by use of Ce3+:LiCaAlF6 as a broadband, solid-state gain medium. Optics Letters. 2002;**26**:301-303. DOI: 10.1364/OL.26.000301

[25] Liu Z, Kozeki T, Suzuki Y, Sarukura N, Shimamura K, Fukuda T, Hirano M, Hosono H. Ce3+: LiCaAlF6 crystal for high-gain or high-peak-power amplification of ultraviolet femtosecond pulses and new potential ultraviolet gain medium: Ce3+: LiSr0:8Ca0:2AlF6. IEEE Journal of Selected Topics Quantum Electronics. 2001;**7**:542-550. DOI: 10.1109/2944.974225

[26] Sarukura N, Dubinskii MA, Liu Z, Semashko VV, Naumov AK, Korableva SL, Abdulsabirov RY, Edamatsu K, Suzuki Y, Segawa T. Ce^{3+}-activated fluoride crystals as prospective active media for widely tunable ultraviolet ultrafast lasers with direct 10-ns pumping. IEEE Journal of Selected Topics Quantum Electronics. 2005;**1**:792-794. DOI: 10.1109/2944.473661

[27] Coutts DW, McGonigle AJS. Cerium-doped fluoride lasers. IEEE Journal of Quantum Electronics. 2004;**40**:1430-1440. DOI: 10.1109/JQE.2004.834775

[28] Pham MH, Cadatal MM, Tatsumi T, Saiki A, Furukawa Y, Nakazato T, Estacio E, Sarukura N, Suyama T, Fukuda K, Kim KJ, Yoshikawa A, Saito F. Laser quality Ce3+: LiCaAlF6 grown by micro-pulling-down method. Japanese Journal of Applied Physics. 2008;**47**:5605-5607. DOI: 10.1143/JJAP.47.5605

[29] Shimamura K, Baldochi SL, Ranieri IM, Sato H, Fujita T, Mazzocchi VL, Parente CBR, Paiva-Santos CO, Santilli CV, Sarukura N, Fukuda T. Crystal growth of Ce-doped and undoped LiCaAlF6 by the Czochralski technique under CF4 atmosphere. Journal of Crystal Growth. 2001;**223**:383-388. DOI: 10.1016/S0022-0248(01)00593-0

[30] Sarukura N, Liu Z, Segawa Y, Semashko VV, Naumov AK, Korableva SL, Abdulsabirov RY, Dubinskii MA. Ultraviolet subnanosecond pulse train generation from an all solid state Ce:LiCAF laser. Applied Physics Letters. 1995;**67**:602-604. DOI: 10.1063/1.115402

[31] Spence DE, Kean PN, Sibbett W. 60-fsec pulse generation from a self-mode-locked Ti: sapphire laser. Optics Letters. 1991;**16**:42-44. DOI: 10.1364/OL.16.000042

[32] Alderighi D, Toci G, Vannini M, Parisi D, Tonelli M. Experimental evaluation of the cw lasing threshold for a Ce:LiCaAlF6 laser. Optics Express. 2005;**13**:7256-7264. DOI: 10.1364/OPEX.13.007256

[33] Granados E, Coutts DW, Spence DJ. Mode-locked deep ultraviolet Ce:LiCAF laser. Optics Letters. 2009;**34**:1660-1662. DOI: 10.1364/OL.34.001660

[34] Roess D. Giant pulse shortening by resonator transients. Journal of Applied Physics. 1966; **37**:2004-2006. DOI: 10.1063/1.1708659

[35] Lin C, Shank CV. Subnanosecond tunable dye laser pulse generation by controlled resonator transients. Applied Physics Letters. 1975;**26**:389-391. DOI: 10.1063/1.88188

[36] Wyatt R. Transient behaviour of pulsed dye lasers. Applied Physics. 1980;**21**:353-359. DOI: 10.1007/BF00895927

[37] Elias LR, Heaps WS, Yen WM. Excitation of UV fluorescence in LaF doped with trivalent cerium and praseodymium. Physical Review B. 1973;**8**:4989-4995. DOI: 10.1103/PhysRevB.8.4989

[38] Yang KH, DeLuca JA. VUV fluorescence of Nd^{3+}, Er^{3+}, and Tm^{3+}-doped trifluorides and tunable coherent sources from 1650 to 2600 A. Applied Physics Letters. 1976;**29**:499-501. DOI: 10.1063/1.89137

[39] Hamilton DS. Trivalent cerium doped crystals as tunable laser systems: Two bad apples. In: Tunable Solid State Lasers. Vol. 47. Berlin: Springer; 1985. pp. 80-90. DOI: 10.1007/978-3-540-39236-1

[40] Lim KS, Hamilton DS. Optical gain and loss studies in Ce3+:YLiF4. Journal of the Optical Society of America B. 1989;**6**:1401-1406. DOI: 10.1364/JOSAB.6.001401

[41] Owen JF, Dorain PB, Kobayasi T. Excited-state absorption in Eu+2:CaF2 and Ce+3:YAG single crystals at 298 and 77 K. Journal of Applied Physics. 1981;**52**:1216-1223. DOI: 10.1063/1.329741

[42] Hamilton DS, Gayen SK, Pogatshnik GJ, Ghen RD. Optical-absorption and photoionization measurements from the excited states of Ce3+:Y3Al5O12. Physical Review B. 1989;**39**:8807-8815. DOI: 10.1103/PhysRevB.39.8807

[43] Pogatshnik GJ, Hamilton DS. Excited-state photoionization of Ce3+ ions in Ce3+:CaF2. Physical Review B. 1987;**36**:8251-8257. DOI: 10.1103/PhysRevB.36.8251

[44] Dubinskii MA, Cefalas AC, Sarantopoulou E, Spyrou SM, Nicolaides CA, Abdulsabirov RY, Korableva SL, Semashko VV. Efficient LaF3:Nd3+-based vacuum-ultraviolet laser at 172 nm. Journal of the Optical Society of America B. 1992;**9**:1148-1150. DOI: 10.1364/JOSAB.9.001148

[45] Rambaldi P, Moncorge R, Wolf JP, Pedrini C, Gesland JY. Efficient and stable pulsed laser operation of Ce:LiLuF4 around 308 nm. Optics Communications. 1998;**146**:163-166. DOI: 10.1016/S0030-4018(97)00519-1

[46] McGonigle AJS, Girard S, Coutts DW, Moncorge R. 10 kHz continuously tunable Ce:LiLuF laser. Electronics Letters. 1999;**35**:1640-1641. DOI: 10.1049/el:19991112

[47] Pinto JF, Rosenblatt GH, Esterowitz L, Quarles GJ. Tunable solid-state laser action in Ce3+:LiSrAlF. Electronics Letters. 1994;**30**:240-241. DOI: 10.1049/el:19940158

[48] Dorenbos P. 5d-level energies of Ce3+ and the crystalline environment. I. Fluoride compounds. Physical Review B. 2000;**62**:15640-15649. DOI: 10.1103/PhysRevB.62.15640

[49] Ono Y, Nakano K, Shimamura K, Fukuda T, Kajitani T. Structural study of colquiriite-type fluorides. Journal of Crystal Growth. 2001;**229**:505-509. DOI: 10.1016/S0022-0248(01)01218-0

[50] Kuze S, Boulay D, Ishizawa N, Kodama N, Yamaga M, Henderson B. Structures of LiCaAlF6 and LiSrAlF6 at 120 and 300 K by synchrotron X-ray single-crystal diffraction. Journal of Solid State Chemistry. 2004;**177**:3505-3513. DOI: 10.1016/j.jssc.2004.04.039

[51] Grzechnik A, Dmitriev V, Weber HP, Gesland JY, Smaalen SV. LiSrAlF6 with the LiBaCrF6-type structure. Journal of Physics: Condensed Matter. 2004;**16**:3005-3013. DOI: 10.1088/0953-8984/16/18/001

[52] Kresse G, Hafner J. Ab initio molecular dynamics for liquid metals. Physical Review B. 1993;**47**:558-561. DOI: 10.1103/PhysRevB.47.558

[53] Kresse G, Hafner J. Ab initio molecular-dynamics simulation of the liquid-metal—-Amorphous-semiconductor transition in germanium. Physical Review B. 1994;**49**:14251-14269. DOI: 10.1103/PhysRevB.49.14251

[54] Kresse G, Furthmuller J. Efficiency of ab-initio total energy calculations for metals and semiconductors using a plane-wave basis set. Computational Materials Science. 1996;**6**:15-50. DOI: 10.1016/0927-0256(96)00008-0

[55] Kresse G, Furthmuller J. Efficient iterative schemes for ab initio total-energy calculations using a plane-wave basis set. Physical Review B. 1996;**54**:11169-11186. DOI: 10.1103/PhysRevB.54.11169

[56] Blochl PE. Projector augmented-wave method. Physical Review B. 1994;**50**:17953-17979. DOI: 10.1103/PhysRevB.50.17953

[57] Kresse G, Joubert D. From ultrasoft pseudopotentials to the projector augmented-wave method. Physical Review B. 1999;**59**:1758-1775. DOI: 10.1103/PhysRevB.59.1758

[58] Perdew J, Burke K, Ernzerhof M. Generalized gradient approximation made simple. Physical Review Letters. 1996;**77**:3865-3868. DOI: 10.1103/PhysRevLett.77.3865

[59] Perdew J, Burke K, Ernzerhof M. Generalized gradient approximation made simple. Physical Review Letters. 1997;**78**:1396. DOI: 10.1103/PhysRevLett.78.1396

[60] Perdew JP, Enzerhof M, Burke K. Rationale for mixing exact exchange with density functional approximations. Journal of Chemical Physics. 1996;**105**:9982-9985. DOI: 10.1063/1.472933

[61] Paier J, Hirschl R, Marsman M, Kresse G. The Perdew-Burke-Ernzerhof exchange-correlation functional applied to the G2-1 test set using a plane-wave basis set. Journal of Chemical Physics. 2005;**122**:234102-234115. DOI: 10.1063/1.1926272

[62] Luong MV, Empizo MJF, Cadatal-Raduban M, Arita R, Minami Y, Shimizu T, Sarukura N, Azechi H, Pham MH, Nguyen HD, Kawazoe Y, Steenbergen KG, Schwerdtferger P. First-principles calculations of electronic and optical properties of LiCaAlF6 and LiSrAlF6

crystals as VUV to UV solid-state laser materials. Optical Materials. 2017;**65**:15-20. DOI: 10.1016/j.optmat.2016.09.062

[63] Shimizu T, Luong MV, Cadatal-Raduban M, Empizo MJF, Yamanoi K, Arita R, Minami Y, Sarukura N, Mitsuo N, Azechi H, Pham MH, Nguyen HD, Ichiyanagi K, Nozawa S, Fukaya R, Adachi S, Nakamura KG, Fukuda K, Kawazoe Y, Steenbergen KG, Schwerdtfeger P. Applied Physics Letters. 2017;**110**:141902. DOI: 10.1063/1.4979106

[64] Setyawan W, Curtarolo S. High-throughput electronic band structure calculations: Challenges and tools. Computational Materials Science. 2010;**49**:299-312. DOI: 10.1016/j.commatsci.2010.05.010

[65] Shiran N, Gektin A, Neicheva S, Weber M, Derenzo S, Kirm M, True M, Shpinkov I, Spassky D, Shimamura K, Ichinose N. Energy transfer in pure and Ce-doped LiCaAlF6 and LiSrAlF6 crystals. Nuclear Instruments and Methods in Physics Research A. 2005; **537**:266-270. DOI: 10.1016/j.nima.2004.08.023

[66] Bensalah A, Shimamura K, Nakano K, Fujita T, Fukuda T. Growth and characterization of LiSrGaF6 single crystal. Journal of Crystal Growth. 2001;**231**:143-147. DOI: 10.1016/S0022-0248(01)01440-3

[67] Shimamura K, Sato H, Bensalah A, Machida H, Sarukura N, Fukuda T. Growth of LiCaAlF single crystals with an extended diameter and their optical characterizations. Journal of Alloys and Compounds. 2002;**343**:204-210. DOI: 10.1016/S0925-8388(02)00125-1

[68] Lawson JK, Payne SA. Excited-state absorption of Eu2+-doped materials. Physical Review B. 1993;**47**:14003-14010. DOI: 10.1103/PhysRevB.47.14003

[69] Schaffers KI, Keszler DA. Structure of LiSrAlF6. Acta Crystallographica. 1991;**C47**:18-20. DOI: 10.1107/S0108270190006205

[70] Liu Z, Ohtake H, Sarukura N, Dubinski M, Semashko VV, Naumov AK, Korableva SL, Abdulsabirov RY. Subnanosecond tunable ultraviolet pulse generation from a low-Q, short-cavity Ce:LiCAF laser. Japanese Journal of Applied Physics. 1997;**36**:L1384-L1386. DOI: 10.1143/JJAP.36.L1384

[71] Liu Z, Sarukura N, Dubinski M, Abdulsabirov RY, Korableva SL. All-solid-state subnanosecond tunable ultraviolet laser sources based on Ce^{3+}-activated fluoride crystals. Journal of Nonlinear Optical Physics and Materials. 1999;**8**:41-54. DOI: 10.1142/S0218863599000047

[72] Meyer YH, BenoistD'azy O, Martin MM, Bréhéret E. Spectral evolution and relaxation oscillations in dye lasers. Optics Communications. 1986;**60**:64-68. DOI: 10.1016/0030-4018(86)90118-5

[73] Hung ND, Segawa Y, Long P, Trung DV. Studies of picosecond spectro-temporal selection lasers using different dyes in microcavities with a two-stage-arrangement. Applied Physics B. 1997;**65**:19-23. DOI: 10.1007/s003400050243

[74] Hung ND, Plaza P, Martin M, Meyer YH. Generation of tunable subpicosecond pulses using low-Q dye cavities. Applied Optics. 1992;**31**:7046-7058. DOI: 10.1364/AO.31.007046

[75] Pham MH, Cadatal-Raduban M, Luong MV, Le HH, Yamanoi K, Nakazato T, Shimizu T, Sarukura N, Nguyen HD. Numerical simulation of ultraviolet picosecond Ce:LiCAF laser emission by optimized resonator transients. Japanese Journal of Applied Physics. 2014;**53**: 062701. DOI: 10.7567/JJAP.53.062701

[76] Ono S, Suzuki Y, Kozeki T, Murakami H, Ohtake H, Sarukura N, Sato H, Machida S, Shimamura K, Fukuda T. High-energy, all-solid-state, ultraviolet laser power-amplifier module design and its output-energy scaling principle. Applied Optics. 2002;**41**:7556-7560. DOI: 10.1364/AO.41.007556